Proc. Natl. Acad. Sci. USA
Vol. 93, pp. 9539–9544, September 1996
Biophysics

Three-dimensional cryoelectron microscopy of dimeric kinesin and ncd motor domains on microtubules

KEIKO HIROSE*†, ANDREW LOCKHART‡, ROBERT A. CROSS‡, AND LINDA A. AMOS*

*Medical Research Council Laboratory of Molecular Biology, Hills Road, Cambridge, CB2 2QH, United Kingdom; and ‡Marie Curie Institute, The Chart, Oxted, Surrey, RH8 0TL, United Kingdom

Communicated by M. F. Perutz, Medical Research Council Laboratory of Molecular Biology, Cambridge, United Kingdom, June 5, 1996 (received for review March 15, 1996)

ABSTRACT **Kinesin and ncd motor proteins are homologous in sequence yet move in opposite directions along microtubules. We have previously shown that monomeric kinesin and ncd bind in the same orientation on equivalent sites relative to the ends of tubulin sheets of known polarity. We now report cryoelectron microscope images of 16-protofilament microtubules decorated with both single- and double-headed kinesin and double-headed ncd. Three-dimensional density maps and difference maps show that, in adenosine 5′-[β,γ-imido]triphosphate, both dimeric motors bind tightly to microtubules via one head, leaving the other free, though apparently in a fixed position. The attached heads of dimers bind to tubulin in the same way as single kinesin heads. The second heads are connected to the tops of the first but, whereas the second kinesin head is closely associated with the first, pairs of ncd heads are splayed apart. There is also a distinct difference in orientation: the second kinesin head is tilted toward the microtubule plus end, while the second head of ncd points toward the minus end.**

Kinesin and ncd belong to a family of proteins that utilize the energy of ATP hydrolysis to move on microtubules (mts). Their directions of motility are opposite: kinesin toward the plus end; ncd toward the minus end (1–3). Both are dimeric molecules with two head domains, a coiled coil rod, and a tail that binds to cargo (4–7). The head (motor) domains expressed in bacterial systems are functional in ATPase and mt binding and translocate mts when properly attached to a surface (8–12). Despite their opposite directions of movement, the motor domains of kinesin and ncd have many similarities: they are homologous in amino acid sequence and atomic structure (13, 14); monomeric constructs of motor domains bind to mts with a stoichiometry of one head per tubulin dimer (9, 10, 15, 16); they compete for binding to equivalent sites on tubulin dimers (16–18); the three-dimensional (3D) structures of tubulin protofilaments (pfs) decorated with monomer kinesin or ncd heads are indistinguishable at low resolution (18–20). How, then, do such similar molecules move in opposite directions?

Both bind to mts tightly in the absence of nucleotide or presence of adenosine 5′-[β,γ-imido]triphosphate (AMP-PNP), and weakly with ADP present (21), though some data suggest the nucleotide specificities of the two motors are not identical (22). We have previously shown by 3D reconstruction of mts decorated with kinesin monomers that a region, assumed to be where the rod and second head of a dimer would connect, points perpendicular to the mt in the presence of ADP but is tilted by ≈45° without nucleotides or in the presence of AMP-PNP (18). These results imply that a domain of the kinesin head changes its angle toward the plus end, in the transition from weakly to strongly bound states. This is consistent with the plus-end-directed movement of kinesin.

If ncd moves by a similar mechanism, one would expect an ncd motor domain to rotate in the opposite direction. However, comparison of 3D maps of ncd (19) and kinesin (18, 20) monomeric motor domains bound to tubulin in the presence of AMP-PNP show no obvious differences, possibly because of limited resolution. Dimeric constructs of kinesin and ncd motor domains may show clear differences, because any angular change in the attached head should be amplified in the position of the tethered head. As a step toward detecting such changes, we have reconstructed 3D images of mts decorated with double-headed kinesin or ncd in the presence of AMP-PNP. The results are strikingly different.

MATERIALS AND METHODS

Kinesin, ncd, and Microtubules. KΔ401, KΔ340 (the first 401 and 340 N-terminal residues of rat kinesin heavy chain) and NΔ295-700 [the C-terminal domain, residues 295–700 of nonclaret disjunctional (ncd), also known as MC5] were prepared and purified as described (16).

To isolate mts with 16 pfs, testes of crickets (*Acheta domesticus*) were dissected, homogenized by a hand homogenizer, suspended in an extracting solution (5 mM Pipes/0.5 mM EGTA/2 mM $MgSO_4$/1 mM DTT/10 μM taxol, pH 7.0), and centrifuged at 150 × *g* for 10 min. The pellet was resuspended in extracting solution and centrifuged at 1000 rpm for 5 min. The supernatant contained sperm tail axonemes released from their heads. Resuspension and centrifugation were repeated several times, and each supernatant was checked by light microscopy. The fractions with the highest axoneme concentration and lowest background were used. For decoration with NΔ295-700, axonemes were prepared in a solution containing phosphate buffer instead of Pipes, to reduce aggregation of the ncd heads.

For decoration with kinesin, the axoneme suspension was mixed with either 4 μM (final) KΔ340 or 5 μM KΔ401, plus 0.5–2 mM AMP-PNP and then applied to an electron microscope grid with a holey carbon film. For decoration with ncd, axonemes were adsorbed to the grid and NΔ295-700 was then added; final concentrations on the grid were 10 μM NΔ295-700, 2 mM AMP-PNP, 5 mM $MgCl_2$.

Electron Microscopy and Image Analysis. Specimens were rapidly frozen by plunging them into ethane slush. Grids were examined using a Gatan cold stage in a Philips EM 420 electron microscope operating at 120 kV and with a defocus of

The publication costs of this article were defrayed in part by page charge payment. This article must therefore be hereby marked "*advertisement*" in accordance with 18 U.S.C. §1734 solely to indicate this fact.

Abbreviations: mt, microtubule; pf, protofilament; KΔ340 and KΔ401, the N-terminal 340 and 401 residues of rat kinesin heavy chain, respectively; NΔ295-700, residues 295 to 700 of *Drosophila* ncd (nonclaret disjunctional protein); AMP-PNP, adenosine 5′-[β,γ-imido]triphosphate; 3D, three dimensional.

†Present address: International Institute for Advanced Research, Matsushita Electric Industrial Co. Ltd., 3-4 Hikaridai, Seika, Kyoto 619-02, Japan.

1300–1600 nm. Electron micrographs taken at a magnification of ×36,000 were digitized in 20-μm steps and processed by standard Fourier methods (see ref. 18). Images of curved mts were straightened and 512 × 1024 Fourier transforms were calculated from 569-nm stretches. Equatorial, 8-nm and 4-nm layer-line data (see Fig. 1) were extracted, to a resolution of about 3.5 nm; as all were within the first zero of the electron microscope contrast transfer function, it was unnecessary to correct for underfocusing. One image provides independent near and far side data, because contributions from different helical families on the nominal layer lines do not overlap. Images with two good sides were selected, since their phase data could be compared, to refine the helix axis and to estimate small tilt angles. Data sets from different images were cross-correlated to find their relative orientations and were rejected if their phase residuals were more than 45°. The 3D maps were finally averaged in real space to facilitate the exclusion of noise outside boundaries and to calculate variance maps. Densities in individual maps were scaled, as described (24), so that the mean density within chosen radial limits was zero and the sum of densities squared (P) was unity. For averages, radial boundaries enclosed the mt and attached motors; for differences between maps of different complexes, the scaling parameters were calculated from mt densities. Values of P were used to select the images for the final averages. Student's t test (25) was used to show whether differences were significant; mean values and standard deviations of averaged maps were compared and the significance of calculated t values was interpreted from a t table.

RESULTS

Microtubule Decoration. Mts were mixed with saturating levels of bacterially expressed motor constructs, namely single- or double-headed kinesin (KΔ340 and KΔ401) or double-headed ncd (NΔ295-700). Optimal conditions for decoration were determined using reassembled brain tubulin and negative stain electron microscopy. For 3D reconstruction, natural mts isolated from cricket testes were imaged in ice; frayed axonemes were photographed (Fig. 2*a*) and 16-pf singlet mts were identified from their diffraction patterns (Figs. 1 and 2 *d* and *e*). Mts decorated with KΔ401 and NΔ295-700 both show the 8-nm tubulin dimer periodicity (Fig. 2), though that for NΔ295-700 was more regular and extended to higher radius.

3D Analysis of 16-Pf Mts. Natural mts with 16 pfs make ideal specimens for image reconstruction because they have perfect helical symmetry. Fig. 2 *d* and *e* show typical diffraction pattern intensities, calculated from digitized images. The patterns due to kinesin or ncd decoration appear identical by eye but density maps, calculated from data including phases and amplitudes, show consistent differences. In each case, 10–15 individual maps, calculated from well-ordered symmetrical Fourier patterns, were compared. A subset that correlated well in real space was averaged to give the final 3D images (Figs. 3 and 4). Sections through the averaged maps and variances among individual maps are included in Fig. 3. The polarity of each complex is clear in cross-section; as established earlier (18), attached heads slew clockwise when viewed from the plus end.

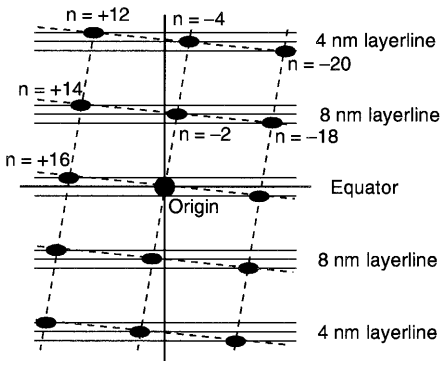

FIG. 1. Diagram showing the reciprocal lattice of a 16-pf mt. The helical lattice of a 16-pf mt is twisted compared with a 13-pf mt to accommodate the extra pfs (23). Hence, in the reciprocal lattice, different contributions to each nominal layer line are at slightly different axial positions. The axial shifts correspond to a longitudinal repeat distance of about 240 nm. The value of n at each point denotes the number of helices in the helical family producing that diffraction peak. Right-handed helices have positive values of n; left-handed are negative.

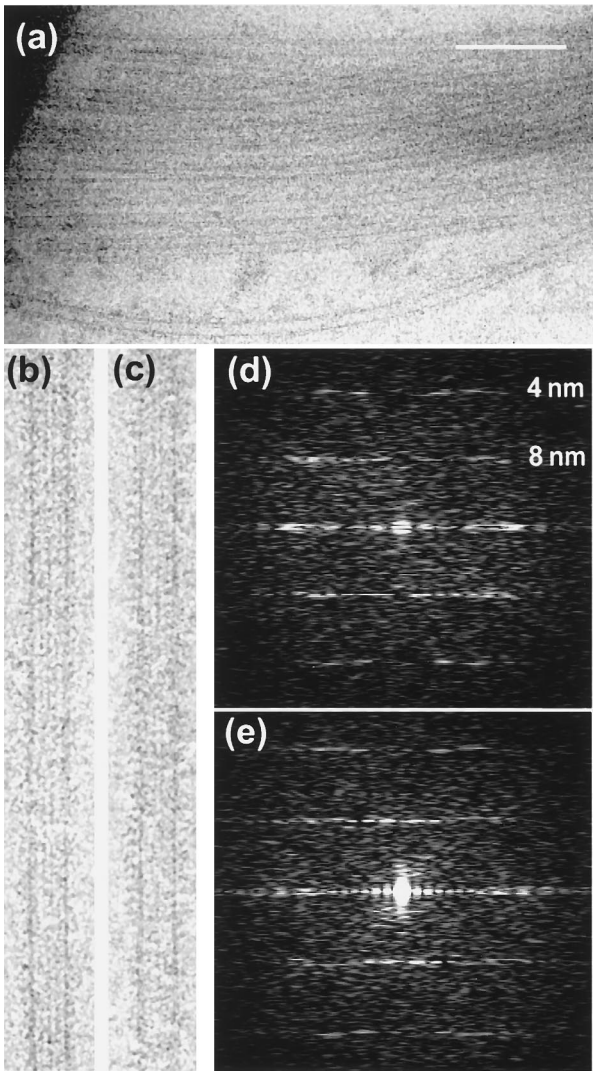

FIG. 2. (*a*) Electron micrograph of mts in a cricket sperm axoneme, embedded in ice over a hole in a carbon film. (Bar = 200 nm.) (*b* and *c*) Images of individual 16-pf mts. In *b* mts are decorated with bacterially expressed double-headed kinesin, KΔ401; in *c* the decoration is double-headed ncd, NΔ295-700. Heads on the right in *c* are less clear than on the left because an adjacent doublet tubule leads to thicker ice. (*d* and *e*) Diffraction patterns computed from digitized images in *b* and *c*; each layer-line is split as in Fig. 1.

KΔ340-Decorated Mts. Density maps of mts decorated with single kinesin heads (Figs. 3*a* and 4*d*) resemble those of negatively stained specimens (18). The heads bind to the left half of the outside surface of a pf but may make a weak contact with the right side of the neighboring pf. On its primary pf, each head contacts two tubulin monomers. In negatively stained specimens, the attached motor appears, in projection, to enhance the upper monomer compared with the lower one

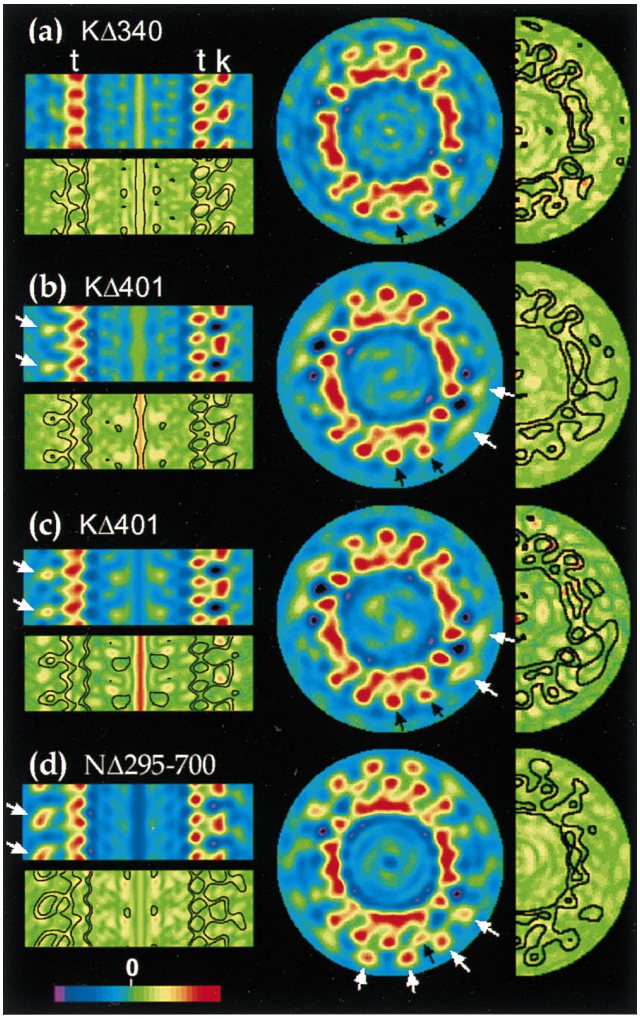

FIG. 3. Sections through averaged 3D maps of protein density and their standard deviations, for mts decorated with single- (*a*) and double- (*b* and *c*) headed kinesin and double-headed ncd (*d*). Maps are normalized (24) to be on the same density scale (see color scale, lower left); the mean density is zero (green). Contours from the density maps are superimposed in black on the error maps. (*a*) An average of four data sets (power in averaged map; $P = 0.73$). (*b*) An average of six data sets ($P = 0.80$). (*c*) An average of the two best KΔ401 data sets ($P = 0.89$). (*d*) An average of five ($P = 0.81$). On the left are vertical sections through the density (*Upper*) and error maps (*Lower*). Each is a composite of two sections through the axis, differing in angle by 192°, so that one passes through a tubulin pf (*t*), the other between pfs but through the centre of the attached heads (*k*). White arrows indicate second heads (absent in *a*). On the right are transverse sections through the density and half sections through error maps. White arrows (*b-d*) indicate sections through second heads. In *a* and *d*, black arrows point to the top section of the first head; in *b* and *c*, larger corresponding peaks include contributions from the second head.

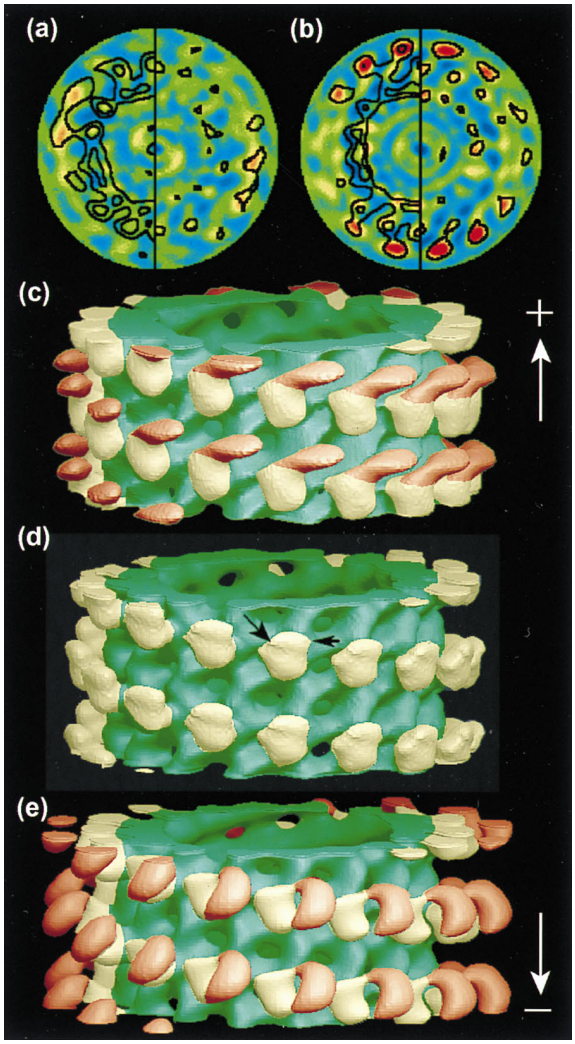

FIG. 4. (*a* and *b*) Horizontal sections through difference maps obtained by subtracting the density of a mt decorated with single-headed KΔ340 from maps with double-headed KΔ401 or NΔ295-700. (The color scale is slightly stretched compared with Fig. 3.) Contours of double-headed motor maps are superimposed over the left half of each difference map. Over the right half, *t*-map contours enclose regions where observed differences have <2% probability of occurring by chance. The difference map shown in *a* is Fig. 3*a* subtracted from Fig. 3*c*, an average of two, but the *t* map was calculated for the difference from Fig. 3*b*, an average of six. (*c–e*) Surface representations of 3D maps for mts decorated with double-headed kinesin (KΔ401: average of two data sets) (*c*), with single-headed kinesin (KΔ340) (*d*), or with double-headed ncd (NΔ295-700) (*e*). The tubulin pfs are colored green, directly attached first heads are cream and tethered second heads are orange. In *d*, the larger arrow indicates a small spike on the kinesin head that may be at the C terminus; the smaller arrow shows the probable location of the N terminus.

(17) but, in ice, both monomers are enhanced equally. Also, the spike (indicated by the larger arrow in Fig. 4*d*) appears slightly further from the mt surface in ice than in negative stain.

KΔ401-Decorated Mts. Density maps for double-headed kinesin (Figs. 3 *b* and *c* and 4*c*) are essentially the same as for KΔ340, apart from additional peaks at outer radii (white arrows in Fig. 3 *b* and *c*). Differences maps (e.g., Fig. 4*a*) have major peaks only in these regions, suggesting that the density peaks here belong to second heads. KΔ401 maps also have some extra density at the tops of the attached heads (black arrows in Fig. 3 *b* and *c*), where the two heads appear to fuse.

The second heads in KΔ401 maps were weaker than expected. Of the individual maps calculated from the six best data sets, two that showed the highest correlation with each other also contained the strongest extra density. The other four maps had density in the same region but it was weaker and more spread out; thus, in the average of all six individual maps (Fig. 3*b*), the density attributed to the second head has a lower value but lies in the same place as in Fig. 3*c*. To check that the difference between single and double-headed kinesin structures is significant, we used Student's *t* test (25). As indicated in Fig. 4*a*, the second head density lies within a contour enclosing points where the observed difference has a probability of 2%, or less, of arising by chance.

NΔ295-700-Decorated Mts. Maps of NΔ295-700-decorated mts showed less variability at the outer radius than KΔ401 maps. Figs. 3*d* and 4*e* show an average of five data sets that

agreed well with each other. A difference map calculated by subtracting the KΔ340 average map from the NΔ295-700 map is shown in Fig. 4*b*; again the strong peaks correspond to putative second heads. The difference map also confirms that attached heads of ncd and kinesin have very similar shapes and bind to mts in a similar manner. The variance map (Fig. 3*d*) suggests the outer head densities in the NΔ295-700 structure are as reliable as those in the attached heads and *t* test calculations show they have a negligible probability of appearing by chance. Some of the weak, less-reliable, density at outer radii in the difference maps (Fig. 4 *a* and *b*) may represent additional lengths of polypeptide in KΔ401 and NΔ295-700, compared with KΔ340, which are probably too thin or disordered to be imaged well.

Comparison of Double-Headed Kinesin and ncd. Surface representations of KΔ401 (Fig. 4*c*) and NΔ295-700 (Fig. 4*e*) both show one head of each dimer attached directly to the mt, while the other is unattached. The attached heads of both dimers are similar to the single head of KΔ340 (Fig. 4*d*), both in shape and in the way they bind to tubulin. Comparison of the difference maps (Fig. 4 *a* and *b*) highlights the differences in the second heads. Although the second head of kinesin is somewhat disordered, the variance maps (Fig. 3) and the estimated significance of the density differences (Fig. 4*a*) suggest that its average position is far from that of the second head of ncd. In the KΔ401-map (Fig. 4*c*), most of the surface of the bulge at the top of the attached head appears to be in close contact with the second head. The two heads of NΔ295-700 are completely separate, apart from a short connection projecting from the top right of the attached head. There is also a clear difference in the orientation of the second heads; the unattached head of a kinesin dimer extends from the top of the first head toward the plus end of the microtubule, while the second head of an ncd dimer extends toward the minus end.

DISCUSSION

Binding Stoichiometry of Double Heads to Mts. Monomeric kinesin and ncd decorate mts with a stoichiometry of one monomer per tubulin dimer (10, 19) but, in the case of double-headed kinesin molecules, there have been binding titration studies suggesting stoichiometries of either one (9) or two (16, 26) heads per tubulin dimer. The situation may vary under different conditions. With no free nucleotide present, only one head releases bound ADP when a dimer binds to a mt (16, 27); but in the presence of AMP-PNP, there is evidence that both heads of the kinesin-like molecule Eg5 can be attached simultaneously, though this state is difficult to stabilize (28). A stoichiometry of one ncd dimer per tubulin dimer is found under all conditions (16, 21).

Experiments herein, as most previous work, included AMP-PNP, which induces strong binding of kinesin and ncd heads to mts (7, 29). The attached heads of KΔ401 or NΔ295-700, which appear in our 3D images to be similar in mass and shape to the heads of KΔ340, occur at 8-nm intervals along each pf, while second heads are unattached. This indicates a stoichiometry of one motor dimer per tubulin dimer but does not exclude the possibility that a small proportion of motor dimers bind via both heads, which would not be seen in the averaged images. The volume of the unattached kinesin head appears a little smaller than the attached head. Binding of some dimers through both heads to sites 8 nm apart would reduce the apparent mass of the unattached head. It would, however, require distortion of one or both heads compared with single bound heads. Since attached heads are similar in our images of single- and double-headed kinesin, it is unlikely that a significant proportion of double-headed molecules had both heads bound. The stoichiometry could be altered by some dimers binding strongly via both heads and breaking into monomers, if the coiled-coil interaction in these constructs is too weak to withstand distortion. However, the most likely cause of low density in the second kinesin head is disorder.

Orientation and Direction of Movement. The shapes of the tubulin pfs are sufficiently polar to confirm that the relative orientations of Fig. 4 *c–e* are correct. Our previous work on tubulin sheets decorated with either kinesin or ncd (17, 18), in which a high density was always superimposed on the tubulin monomer at the plus ends of sheets, indicates that the two motors bind to equivalent sites on α/β-tubulin dimers. This conclusion agrees with competition experiments (16). Since the orientations of bound heads are also the same, we can exclude models in which kinesin and ncd move in opposite directions by binding to mts in opposite orientations.

In 3D images of negatively stained complexes, we identified a short projection or spike from near the top left of the attached head (18). Since the end of the spike was the most distal point observed from the mt surface, it seemed likely to represent the point where the rod would attach in a complete molecule. The spikes are less obvious in images showing single kinesin heads in ice (Fig. 4*d*) but it is clear from the double-headed molecules (Fig. 4 *c* and *e*) that the connections to both types of rod must lie at the tops of attached heads.

We also saw earlier that the spike from KΔ340 changed angle in a nucleotide-dependent way: it appeared to lie normal to the mt axis when kinesin was occupied by ADP but was tilted toward the mt plus end in the absence of nucleotide or presence of AMP-PNP (18). The observed change supports the idea that motility results from angular changes of the bound head and is consistent with kinesin's movement toward the plus ends of mts. In the case of ncd, there is as yet no information regarding conformational changes between different nucleotide states.

Relative Orientations of Motor Polypeptides. In complete molecules, the C terminus of a kinesin head or the N terminus of an ncd head is connected to a coiled-coil rod. The ncd rod must emerge from the narrow bridge of density seen connecting the two heads in the 3D map (Fig. 4*e*); thus the N terminus of the motor domain should be at the top right of the attached head (smaller arrow in Fig. 4*d*). The position of the C-terminal connection between kinesin heads is less well defined, as the two heads appear to be quite closely apposed. However, the shape of the molecule is consistent with the two heads being connected by a tail domain that emerges from left of the top center of the attached head. The crystal structures of kinesin and ncd head domains (13, 14) also suggest that the N and C termini of each polypeptide are fairly close, although some terminal residues are unseen. Stewart *et al.* (11) showed that the direction in which kinesin moves does not depend on whether the head is attached via the N or C terminus. This result could be explained, without conflicting with models in which structural changes of the head produce motility, if N and C termini lie close together.

Motile Mechanisms. It has been suggested that the two heads of a kinesin molecule interact with tubulin alternately, thus moving along mts in a hand-over-hand fashion (12, 27, 30, 31). The track on which kinesin moves is parallel to the pf axis (32). Although single kinesin heads are capable of producing force, the double-headed structure is needed for pf tracking (12). For such a precise mechanism to work, potential binding sites for the unattached head must be restricted by the conformation of the attached head. It is not clear whether ncd heads cooperate similarly, but the fixed angle of the free head makes this likely. The simplest model is to have the attached heads change conformation in opposite ways, so that the unattached heads are pulled closer to the plus end in case of kinesin but toward the minus end with ncd. The most important finding in this paper is that, in a strongly bound state, the positions of unattached heads are indeed different: the second head of kinesin is closer to the plus end of the mt, whereas the

second head of ncd is level with the attached head and points toward the minus end.

Models have been suggested in which a motor follows a pf either with each head finding the next subunit on the same pf or with two heads using neighboring pfs (16, 33). Because the two heads are identical and the connection between them behaves as a flexible hinge, we expect the relative positions of the original and next binding sites to be essentially identical after every step. Thus, we prefer the first model. In the 3D images (Fig. 4 *c* and *e*), it means that an unattached head, colored orange, has to replace the attached cream-colored head of the next molecule above (kinesin) or below (ncd).

Compared with KΔ340, KΔ401 has 61 extra amino acids, mostly predicted to be capable of forming coiled-coil (11, 34); NΔ295-700 has a corresponding region near its N terminus. A model has been suggested (26) in which part of the coiled-coil reversibly unravels, which would make the lever arm longer and allow the unattached head to reach the next binding site. A model based on our images of two-headed kinesin and coiled-coil unraveling is illustrated in Fig. 5*a*. Alternative models could involve conformational changes within the head domain, making it longer, or the leading head might bind transiently to an intermediate site on tubulin. The model for ncd movement (Fig. 5*b*) is more tentative, since we do not know whether ncd tilts in the opposite direction to kinesin during ADP release or another step in the kinetic cycle. The state imaged here may not be the one in which the attached head is most tilted toward the minus end. However, our results show that when dimeric motors are tightly bound to the mt by one head, the positions of the unattached heads are biased toward the direction of movement. The positions seen for kinesin should increase the probability of finding a new site closer to the plus end and for ncd a site nearer the minus end. We think that this could at least partly explain the opposite direction of movement of these molecules.

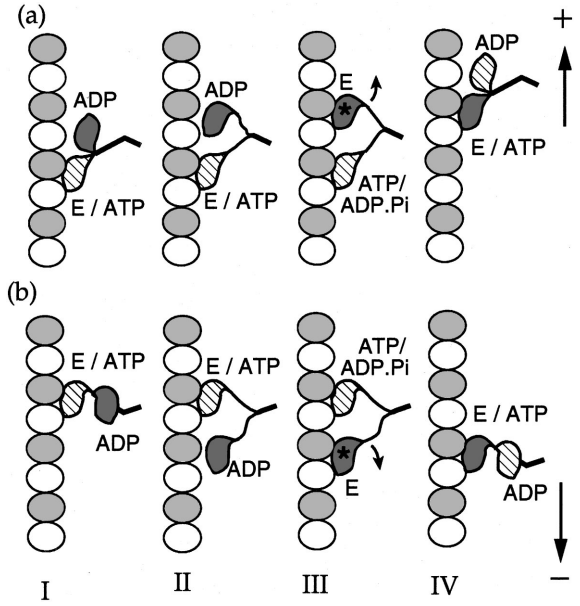

FIG. 5. (*a*) Model of a mechanism by which a pair of kinesin heads might alternately attach to and detach from a tubulin pf to produce movement. We showed (18) that the most distal part of an attached head tilts toward the plus end of the mt after ADP release. It is then (stage I) in a strongly bound state [labeled E/ATP (nucleotide site empty or containing fresh ATP)]. If there is close association between the heads, as in the 3D images, the second (now leading) head cannot easily reach and bind to the next site on the pf. Part of the coiled-coil connecting the heads may unzip temporarily (26), allowing the second head to reach the new site (stage II). Meanwhile, the first head binds and hydrolyses a fresh molecule of ATP. It is unclear how (*i*) binding of ATP to the rear head and its hydrolysis and the subsequent release of the rear head and (*ii*) the attachment of the leading head to the pf and ADP release are coordinated, except that each occupy half the cycle time (35). To adapt the current best model (36), we propose that the leading head can lose its bound ADP during random contact with the new site and thereby become strongly bound but cannot tilt forward while the rear head remains strongly attached (stage III—the asterisk indicates a state of tension in this molecule). The rear head binds a fresh molecule of ATP, hydrolyses it, and converts to a weakly bound state. Then the tension produced by the leading head can pull the rear head forward (stage IV). (*b*) An equivalent model for ncd, assuming that ncd also moves processively and that the distal part of the head tilts in the opposite direction to kinesin after releasing ADP.

We thank Drs. Richard Henderson, Nigel Unwin, and Chikashi Toyoshima for help with cryoelectron microscopy techniques; Dr. Brad Amos for help in obtaining cricket testes; Dr. Juan Fan for purified brain tubulin; Drs. Anne Sperry and Scott Brady for the rat kinesin heavy chain clone; and Dr. Sharyn Endow for the *Drosophila* ncd clone.

1. Goldstein, L. S. B. (1993) *Annu. Rev. Genet.* **27,** 319–351.
2. Walker, R. A. & Sheetz, M. P. (1993) *Annu. Rev. Biochem.* **62,** 429–451.
3. Walker, R. A., Salmon, E. D. & Endow, S. A. (1990) *Nature (London)* **347,** 780–782.
4. Hirokawa, N., Pfister, K. K., Yorifuji, H., Wagner, M. C., Brady, S. T. & Bloom, G. S. (1989) *Cell* **56,** 867–878.
5. Scholey, J. M., Heuser, J., Yang, J. T. & Goldstein, L. S. B. (1989) *Nature (London)* **338,** 355–357.
6. Yang, J. T., Laymon, R. A. & Goldstein, L. S. B. (1989) *Cell* **56,** 879–889.
7. Chandra, R., Salmon, E. D., Erickson, H. P., Lockhart, A. & Endow, S. A. (1993) *J. Biol. Chem.* **268,** 9005–9013.
8. Yang, J. T., Saxton, W. M., Stewart, R. J., Raff, E. C. & Goldstein, L. S. B. (1990) *Science* **249,** 42–47.
9. Harrison, B. C., Marchese-Ragona, S. P., Gilbert, S. P., Cheng, N., Steven, A. C. & Johnson, K. A. (1993) *Nature (London)* **362,** 73–75.
10. Huang, T. G. & Hackney, D. D. (1994) *J. Biol. Chem.* **269,** 16493–16501.
11. Stewart, R. J., Thaler, J. P. & Goldstein, L. S. B. (1993) *Proc. Natl. Acad. Sci. USA* **90,** 5209–5213.
12. Berliner, E., Young, E. C., Anderson, K., Mahtani, H. K. & Gelles, J. (1995) *Nature (London)* **373,** 718–721.
13. Kull, F. J., Sablin, E. P., Lau, R., Fletterick, R. J. & Vale, R. D. (1996) *Nature (London)* **380,** 550–555.
14. Sablin, E. P., Kull, F. J., Cooke, R., Vale, R. D. & Fletterick, R. J. (1996) *Nature (London)* **380,** 555–559.
15. Song, Y.-H. & Mandelkow, E. (1993) *Proc. Natl. Acad. Sci. USA* **90,** 1671–1675.
16. Lockhart, A., Crevel, I. M.-T. C. & Cross, R. A. (1995) *J. Mol. Biol.* **249,** 763–771.
17. Hirose, K., Fan, J. & Amos, L. A. (1995) *J. Mol. Biol.* **251,** 329–333.
18. Hirose, K., Lockhart, A., Cross, R. A. & Amos, L. A. (1995) *Nature (London)* **376,** 277–279.
19. Hoenger, A., Sablin, E. P., Vale, R. D., Fletterick, R. J. & Milligan, R. A. (1995) *Nature (London)* **376,** 271–274.
20. Kikkawa, M., Ishikawa, T., Wakabayashi, T. & Hirokawa, N. (1995) *Nature (London)* **376,** 274–279.
21. Crevel, I. M.-T., Lockhart, A. & Cross, R. A. (1996) *J. Mol. Biol.* **257,** 66–76.
22. Shimizu, T., Sablin, E., Vale, R. D., Fletterick, R., Pechatnikova, E. & Taylor, E. W. (1995) *Biochemistry* **34,** 13259–13266.
23. Wade, R. H., Chrétien, D. & Job, D. (1990) *J. Mol. Biol.* **212,** 775–786.
24. Trachtenberg, S. & DeRosier, D. J. (1987) *J. Mol. Biol.* **195,** 581–601.
25. Milligan, R. A. & Flicker, P. F. (1987) *J. Cell Biol.* **105,** 29–39.
26. Huang, T. G., Suhan, J. & Hackney, D. D. (1994) *J. Biol. Chem.* **269,** 16502–16507.
27. Hackney, D. D. (1994) *Proc. Natl. Acad. Sci. USA* **91,** 6865–6869.
28. Lockhart, A. & Cross, R. A. (1996) *Biochemistry* **35,** 2365–2373.
29. Romberg, L. & Vale, R. D. (1993) *Nature (London)* **361,** 168–170.
30. Howard, J., Hudspeth, A. J. & Vale, R. D. (1989) *Nature (London)* **342,** 154–158.

31. Hackney, D. D. (1995) *Nature (London)* **377,** 448–450.
32. Ray, S., Meyhöfer, E., Milligan, R. A. & Howard, J. (1993) *J. Cell Biol.* **121,** 1083–1093.
33. Howard, J. (1995) *Biophys. J.* **68,** 245s–255s.
34. Young, E. C., Berliner, E., Mahtani, H. K., Perezramirez, B. & Gelles, J. (1995) *J. Biol. Chem.* **270,** 3926–3931.
35. Ma, Y. Z. & Taylor, E. W. (1995) *Biochemistry* **34,** 13242–13251.
36. Peskin, C. S. & Oster, G. (1995) *Biophys. J.* **68,** 202s–211s.